[4]Ashley H., and Rowe, W. S., "Unsteady Aerodynamic Loading of Wings with Control Surfaces," *Z. Flugwissenschaften*, Vol. 18 Sept./Oct., 1970, pp. 321–330.

[5]Kussner H. G., "General Lifting Surface Theory," *Luftfahrtforschung*, Vol. 17, No. 11/12, Dec. 1940.

[6]Watkins, C. E., Runyan, H. L. and Woolston, D. S., "On the Kernel Function of the Integral Equation Relating the Lift and Downwash Distributions of Oscillating Finite Wings in Subsonic Flow," NACA Rep. 1234, 1955.

[7]Hsu P. T., "Calculation of Pressure Distributions for Oscillating Wings of Arbitrary Planform in Subsonic Flow by the Kernel Function Method," MIT ASRL T.R. 64-1, Oct. 1957.

[8]Multhopp, H., "Methods for Calculating the Lift Distribution of Wings (Subsonic Lifting-Surface Theory)," Aeronautical Research Council R-M 2884, Jan. 1950.

[9]Laschka B., "Zur Theorie der Harmonish Schwingenden Tragenden Flache bez Unterschallstromung," *Z. Flugwissenschaften*, Vol. 12, 1963, pp. 265–292.

[10]Hammond A. D. and Keffer B. A., "The Effect at High Subsonic Speeds of a Flap-Type Aileron on the Chordwise Pressure Distribution Near Midsemispan of a 35° Sweptback Wing of Aspect Ratio 4 having NACA 65A006 Airfoil Section," NACA RM L53C23, March 1953.

[11]Forsching, H., Triebstein, H., and Wagener J., "Pressure Measurements on Harmonically Oscillating swept Wing with Two Control Surfaces in Incompressible Flow," AVA FB 7025, 1970, AGARD Symposium, Tonsberg, Norway.

[12]Abbott I. H. and VonDoenhoff A. E., "Theory of Wing Sections," McGraw-Hill, New York, 1949.

JANUARY 1974 J. AIRCRAFT VOL. 11, NO. 1

Flowfield Analysis for Successive Oblique Shock Wave-Turbulent Boundary-Layer Interactions

Chen-Chih Sun* and Morris E. Childs†
University of Washington, Seattle, Wash.

A computation procedure is described for predicting the flowfields which develop when successive interactions between oblique shock waves and a turbulent boundary layer occur. Such interactions may occur, for example, in engine inlets for supersonic aircraft. Computations have been carried out for axisymmetric internal flows at $M_\infty = 3.82$ and 2.82. The effect of boundary layer bleed has been considered for the $M_\infty = 2.82$ flow. A control volume analysis is used to predict changes in the flow field across the interactions. Two bleed flow models have been considered. A turbulent boundary layer program has been used to compute changes in the boundary layer between the interactions. The results given are for flows with two shock wave interactions and for bleed at the second interaction site. In principle the method described may be extended to account for additional interactions. The predicted results are compared with measured results and are shown to be in good agreement when the bleed flow rate is low (on the order of 3% of the boundary layer mass flow), or when there is no bleed. As the bleed flow rate is increased, differences between the predicted and measured results become larger. Shortcomings of the bleed flow models at higher bleed flow rates are discussed.

Nomenclature

A = $\{[(\gamma-1)/2]\, M_e^2/(T_w/T_e)\}^{1/2}$
a = a constant in the wall-wake profile
B = $\{(1+[(\gamma-1)/2]M_e^2)/(T_w/T_e)\} - 1$
C = a constant in the Law of the Wall (usually equals 5.1)
C_f = skin friction coefficient, $\tau_w/(1/2)\rho_e u_e^2$
I_{Bx} = x-momentum of the bleed flow
K = a constant in the Law of the Wall (usually equals 0.4)
L = shock wave-boundary layer interaction length
M = Mach number
$\dot{m}_B$ = boundary layer mass bleed rate
P = pressure
R = radial coordinate from tunnel centerline
R_B = radial coordinate of dividing stream surface separating bleed flow from main flow, (see Fig. 3)
Re = Reynolds number
u = velocity in streamwise direction
u^* = van Driest's generalized velocity, $(u_e/A)\arcsin\{[(2A^2u/u_e) - B]/(B^2+4A^2)^{1/2}\}$
u_τ = friction velocity, $(\tau_w/\rho_w)^{1/2}$
x = axial coordinate, measured from shock generator tip
y = coordinate normal to the tunnel wall
γ = ratio of specific heats
Δ_E = a thickness of freestream flow to allow for boundary layer mass entrainment, (see Fig. 3)
δ = boundary layer thickness
δ^* = displacement thickness of the boundary layer
η = y/δ
θ = momentum thickness of the boundary layer
ν = kinematic viscosity
Π = coefficient of the wake function
ρ = mass density
σ = $[(\gamma-1)/2]M_e^2/\{1+[(\gamma-1)/2]M_e^2\}$
τ = shear stress

Subscripts

e = conditions at the edge of the boundary layer
w = conditions at the wall
∞ = freestream conditions ahead of the first interaction

Received April 23, 1973; revision received October 29, 1973. This work was supported by NASA Grant NGR-48-002-047 under administration of the Aerodynamics Branch, Ames Research Center.

Index categories: Boundary Layers and Convective Heat Transfer—Turbulent; Supersonic and Hypersonic Flow; Shock Waves and Detonations.

*Research Associate (Postdoctoral), Department of Mechanical Engineering.

†Professor of Mechanical Engineering. Member AIAA.

Introduction

THE interaction of an oblique shock wave with a turbulent boundary layer is known to induce drastic changes in the boundary-layer properties and to cause substantial de-

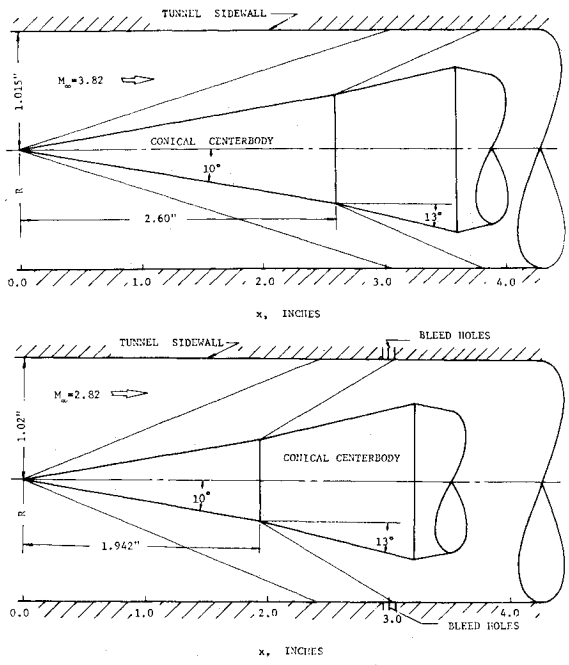

Fig. 1 Experimental configuration.

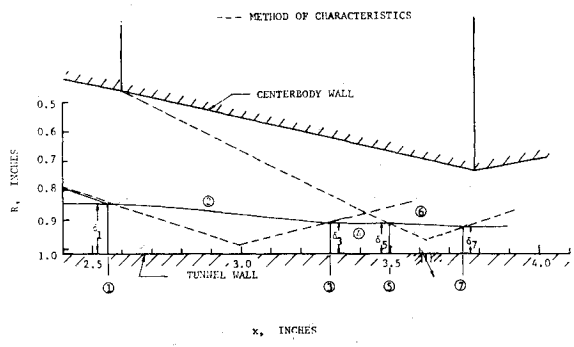

Fig. 2 Flow model used in analysis.

viation of the supersonic flowfield from the predicted inviscid flow. This deviation may be of sufficient magnitude to adversely affect the performance of aerodynamic devices. Suitable methods for predicting the boundary-layer and freestream flow characteristics in the presence of such disturbances are required by engineers responsible for the design of aerodynamic configurations involving shock wave boundary-layer interactions.

A control volume method developed by Seebaugh, Paynter and Childs,[1] and improved upon by Mathews,[2] has been successful in the prediction of boundary layer characteristics downstream of the interaction with a single oblique shock wave. However, in some aerodynamic devices, such as mixed compression supersonic diffusers, the turbulent boundary layer is often subjected to interactions with more than one shock wave. In the study reported here the control volume method has been used to calculate the changes in turbulent boundary layer characteristics across successive shock wave interactions at the walls of axisymmetric wind tunnels. Two cases are reported, one at $M_\infty = 2.82$, the other at $M_\infty = 3.82$. In the Mach 2.82 study the effect of boundary layer bleed at the second interaction site was considered. A turbulent boundary layer computer program was used to predict boundary layer changes between the two interactions and to provide the initial conditions for the second interaction.

Experimental Configurations

The experimental configurations which were used to produce the successive shock waves are shown schematically in Fig. 1. The Mach 3.82 tunnel had a radius of 1.015 in. and a boundary layer thickness ahead of the first interaction of 0.170 in. The shock wave generator was installed on the centerline of the tunnel at zero angle of attack. The generator had a 10° half-angle conical tip which broke to 13° 2.60 in. downstream of the tip. For the Mach 2.82 tunnel the tunnel radius was 1.02 in., and the boundary layer thickness ahead of the first interaction was 0.165 in. The shock generator had a 10° conical tip which broke to 13° 1.942 in. behind the tip. Both generators were designed to provide as large a region of freestream flow as possible between the first reflected and second incident shock waves while at the same time keeping the expansion wave off the downstream corner of the second conical surface from interfering with the second interaction.

About 3.0 in. from the tip of the Mach 2.82 shock generator, or approximately at the point where the second incident shock wave reached the wall, two rows of thirty-eight 0.052-in. diam bleed holes were drilled around the periphery of the tunnel. The bleed system was operated in a choked flow condition. With one row of the holes open, the bleed mass flux was about 2.8% of the boundary layer mass flux just ahead of the second interaction. With two rows of holes open, the bleed mass flux was 5.0% of the boundary layer mass flux.

Both tunnels were operated with a steady supply of dry air at 540°R. The freestream unit Reynolds number for the $M = 3.82$ tunnel was 5.62×10^6/ft, that for the $M = 2.82$ tunnel, 5.8×10^6/ft.

Instrumentation

Standard instrumentation was used to obtain tunnel wall static pressures and boundary layer pitot pressure profiles. Wall static pressures were taken at 0.05-in. intervals along the tunnel sidewalls. Pitot profiles were taken in radial increments of 0.005 in. at 18 axial stations upstream of, within, and downstream of the interaction region. Miniature total head tubes, flattened to a dimension of 0.009 in. high × 0.026 in. wide were used for the pitot profiles. Velocity profiles upstream of the first incident shock wave, between the first reflected and second incident shock waves, and downstream of the second reflected shock wave were calculated from the pitot profiles assuming isoenergetic flow and constant static pressure across the boundary layer. A calibrated venturi meter was used to measure the bleed flow rate.

Analysis

Figure 2 shows the flow model used in the analysis. R is the radial distance from the tunnel centerline and x is the distance downstream from the tip of the generator. Conditions at the Station 1 are assumed to be known. The object of the analysis, given the shock generator shape and position, is to compute the locations of the reflected shock waves and the boundary layer properties at successive stations along the wall.

The computation is carried out in three steps associated with three subregions into which the boundary layer flow is divided.

1) *Region I* extends from Station 1 where the first incident shock wave reaches the boundary-layer edge to Station 3 where the reflected shock wave emerges from the boundary layer. Surface 2 is the stream surface which passes through the intersection of the incident conical shock with the boundary layer edge. The location of this surface and the pressure distribution along it are obtained from an inviscid conical flow solution. Using this surface, the tunnel wall, and the planes normal to the wall at 1

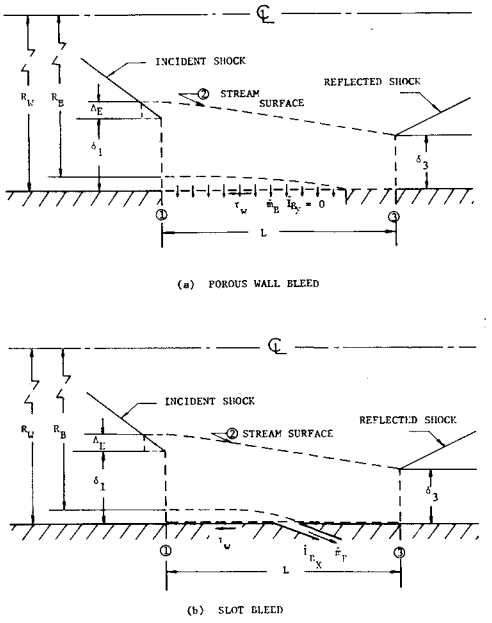

Fig. 3 Control volumes used in analysis.

and 3 to define a control volume, a control volume analysis of the region may be used to determine the length of the interaction, and the boundary layer thickness and shape at 3. In the analysis by Seebaugh, Paynter and Childs[1] the method of solution was as follows. The velocity profile at Station 1 was represented by a least-squares-fit power-law profile. The downstream boundary-layer thickness and power-law profile were then obtained by solving the continuity and x-momentum equations for the control volume. The interaction length, which is related to δ_3 by the geometry of the edge stream surface, was determined in the solution. In the analysis, the pressure at 3 was taken to be the wall static pressure at Station 3 as determined from an inviscid flow solution. The wall shear force was neglected and mass entrainment into the boundary layer through the interaction was ignored.

In a subsequent analysis Mathews[2,3] used a law-of-the-wall/law-of-the-wake profile to replace the power-law profile for representing the velocity distribution upstream and downstream of the interaction. In Mathews' analysis the value of C_{f1} at Station 1 was known from a least-squares fit of the wall-wake profile to the upstream velocity profile. A tentative value of C_{f3} was then determined by a control volume analysis for a two-dimensional interaction. This made it possible to take the shear force on the wall into consideration in an approximate way, i.e., by using an average of C_{f1} and C_{f3} to give an average wall shear stress. This scheme should be reasonably good for weak interactions but will overpredict the effect of wall shear as the shock strength is increased, and a condition of flow separation is approached. Taking the tentative value of C_{f3} as determined in the two-dimensional control volume analysis as the initial estimate of C_{f3}, an iterative technique was then used to obtain the final value for C_{f3} and an average wall shear stress. Mathews also allowed for boundary-layer mass entrainment in the interaction region in an approximate way by taking it to be equal to the entrainment rate ahead of the interaction. His experimental results supported this assumption. For interactions of weak to moderate strength, Mathews' analysis led to somewhat better agreement between predicted and measured downstream boundary properties than had been obtained in the Seebaugh analysis.

In the analysis used to predict the results reported here, additional modifications to the control volume analysis have been made. Recently, Sun and Childs[4] have developed an improved wall-wake velocity profile for turbulent isoenergetic compressible boundary-layer flow. The modified profile may be expressed in the form

$$\frac{u}{u_e} = \frac{(B^2+4A^2)^{1/2}}{2A^2}\sin\left\{\arcsin\left(\frac{2A^2-B}{B^2+4A^2)^{1/2}}\right)\left[1 + \frac{1}{K}\frac{u_\tau}{u_e{}^*}\left(\ln\eta + \frac{2}{a}(1-\eta^a)^{1/2} - \frac{2}{a}\ln(1+(1-\eta^a)^{1/2})\right) - \frac{\Pi}{K}\frac{u_\tau}{u_e{}^*}(1+\cos\eta\pi)\right]\right\} + \frac{B}{2A^2} \quad (1)$$

or

$$\frac{u}{u_e} = \frac{1}{\sigma^{1/2}}\sin\left\{\arcsin\sigma^{1/2}\left[1 + \frac{1}{K}\frac{u_\tau}{u_e{}^*}\left(\ln\eta + \frac{2}{a}(1-\eta^a)^{1/2} - \frac{2}{a}\ln\left(1+(1-\eta^a)^{1/2}\right)\right) - \frac{\Pi}{K}\frac{u_\tau}{u_e{}^*}(1+\cos\eta\pi)\right]\right\} \quad (2)$$

where

$$\Pi/K = (1/2)\{(u_e{}^*/u_\tau) - (1/K)\ln(\delta u_\tau/\nu_w) - 5.1 + 0.614/aK\} \quad (3)$$

A least squares fit of the velocity profile given by Eq. 2 to experimental data gives values of δ and u_τ or C_f. For $a \to \infty$, Eq (2) reduces to the velocity profile used by Mathews in his analysis. While Mathews' profile has been found to provide a good representation of turbulent compressible boundary-layer velocity profiles, it does have the shortcoming that the velocity gradient does not go to zero at $y = \delta$. With $a = 1$, on the other hand, this shortcoming is avoided. Furthermore, more realistic values of δ, i.e., nearer the values corresponding to $u/u_e = 0.99$, are found when $a = 1$. In the results reported here the velocity profiles have been assumed to be given by the modified wall-wake profile with $a = 1$.

One other variation on the earlier methods has been incorporated into the present analysis. Namely, the flow direction in the boundary-layer downstream of the interaction has been taken as the average of the value at the wall (i.e., zero) and at $y = \delta_3$, as determined from the inviscid solution. The pressure at 3 has then been based on the average flow direction. In the analyses by Seebaugh and Mathews the flow direction downstream of an interaction was taken to be parallel to the wall.

Figures 3a and 3b show the control volumes used in the present analysis. Although boundary-layer bleed was not employed at the first interaction site, the control volumes shown do allow for that possibility. For the control volumes shown, the continuity equation may be expressed in the form

$$\int_{R_W-\delta_1-\Delta_E}^{R_W} 2\pi\rho u R dR = \int_{R_W-\delta_3}^{R_W} 2\pi\rho u R dR + \dot{m}_B$$

while the x-momentum equation may be written as:

$$\int_{R_W-\delta_1-\Delta_E}^{R_W} 2\pi P_1 R dR - \int_{R_W-\delta_1-\Delta_E}^{R_W-\delta_3} 2\pi P_2 R dR - \int_{R_W-\delta_3}^{R_W} \bar{P}_3 2\pi R dR - 2\pi R_w L\bar{\tau}_w = \int_{R_W-\delta_3}^{R_W} 2\pi\rho u^2 R dR - \int_{R_W-\delta_1-\Delta_E}^{R_W} 2\pi\rho u^2 R dR + I_{B_x}$$

where $\bar{\tau}_w = (\tau_{w1} + \tau_{w3})/2$ and $\bar{P}_3$ is the average static pressure over the boundary layer at 3. With suitable representation of the magnitude of I_{bx} and with the assumption that the velocity profile at 3 is given by Eq. (2), the equations may be solved for L, δ_3 and the profile shape at 3. Comparable equations may be written for the second interaction site.

In the control volume equations given above the conditions at the beginning of the interaction, as well as the

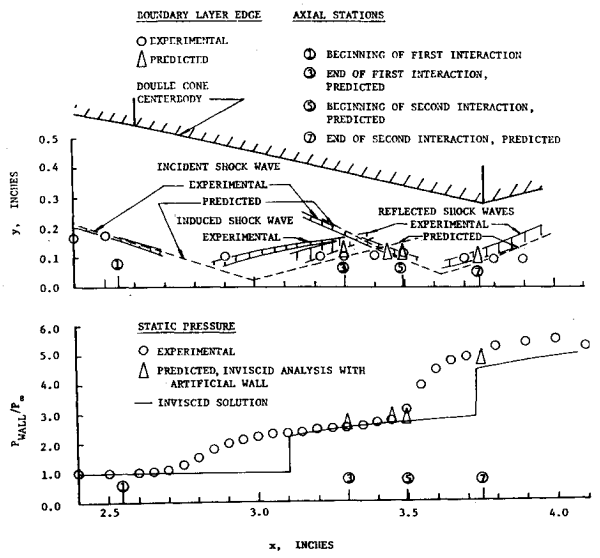

Fig. 4 Shock wave positions, boundary-layer thicknesses and wall static pressures, $M_\infty = 3.82$, no bleed.

mass bleed rate, $\dot{m}_B$, are assumed to be known. Conditions along surface 2 are determined from an inviscid flow analysis for the given tunnel and shock generator geometry.

The x-momentum of the bleed flow depends on the manner in which the bleed flow is accomplished. In the analyses by Seebaugh[1] and Mathews[2] computations were made for three bleed models: porous-wall suction, slot suction and scoop suction. Figure 3a shows the porous wall model. With this model, the x-momentum of the bleed flow, I_{Bx}, was assumed to be zero. Figure 3b shows the slot-suction model. With slot suction, $\dot{I}_{Bx}$ was assumed to have the same value as that possessed by the bleed mass as it entered the control volume, i.e.,

$$\dot{I}_{B_x} = \int_{R_B}^{R_w} 2\pi\rho u^2 R dR$$

where R_B is determined from

$$\dot{m}_B = \int_{R_B}^{R_w} 2\pi\rho u R dR$$

2) *Region II* extends from Station 3 to Station 5. This is the region of boundary-layer flow between the first reflected shock and the second incident shock. Since no shock

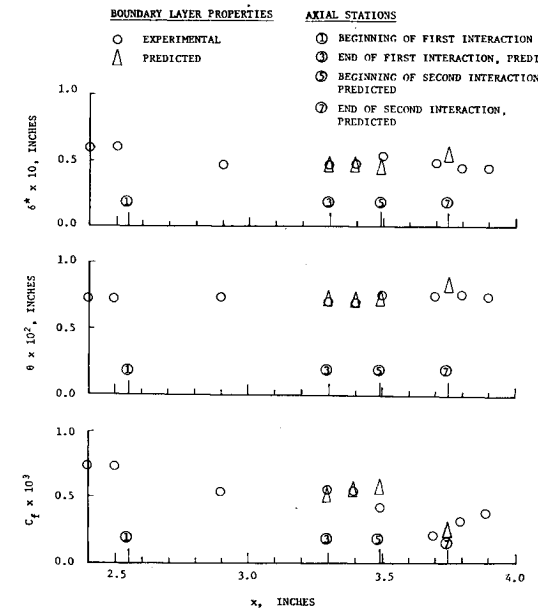

Fig. 5 δ^*, θ, and C_f, $M_\infty = 3.82$, no bleed.

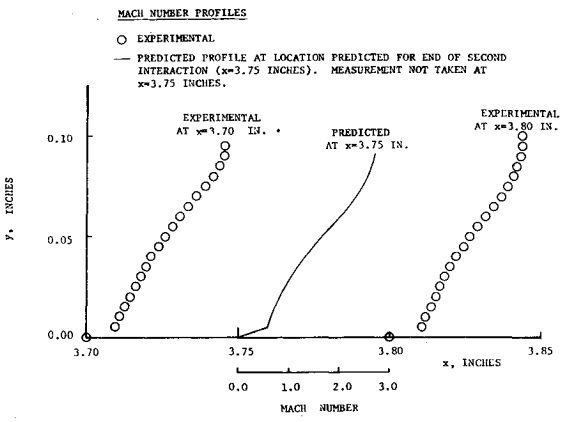

Fig. 6 Mach number profiles downstream of second interaction, $M_\infty = 3.82$, no bleed.

interactions are present in this region, the axial pressure gradient is relatively low. Starting with conditions at 3 as determined by the control volume analysis of the first interaction, changes in the boundary-layer properties to Station 5 are computed using a turbulent boundary layer program suggested by Paynter and Schuehle.[5] The program uses a wall-wake profile[4] to represent the velocity profile and the entrainment function concept proposed by Green[6] to solve the boundary-layer equations. An inviscid flow solution is used to provide the wall static pressure distribution needed for the boundary-layer solution in this region. The inviscid solution, however, was obtained in a manner which allowed for the effects of the first shock interaction. The method employed was to use an artificial wall position in the interaction region which would cause the reflected inviscid shock wave position to match that determined by the control volume analysis.

3) *Region III* extends from Station 5 to Station 7. This region covers the interaction of the second incident shock wave with the boundary layer. The method here is similar to that for Region I, except that the flow at control surface 6 is no longer conical. Conditions along this surface were obtained from a method of characteristics solution for flow past the double-cone centerbody. In the characteristics solution the interaction of the first reflected shock with the second incident shock must be considered. The location in the flowfield of the reflected shock was determined using the artificial wall position.

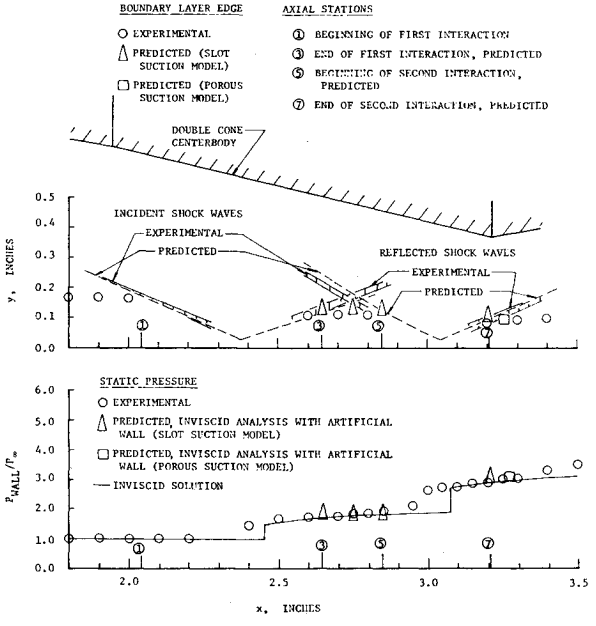

Fig. 7 Shock wave positions, boundary-layer thicknesses and wall static pressures, $M_\infty = 2.82$, 2.8% bleed.

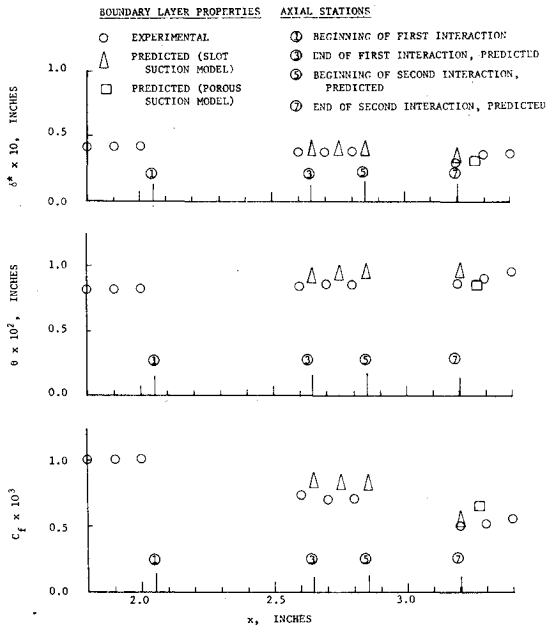

Fig. 8 δ^*, θ, and C_f, $M_\infty = 2.82$, 2.8% bleed.

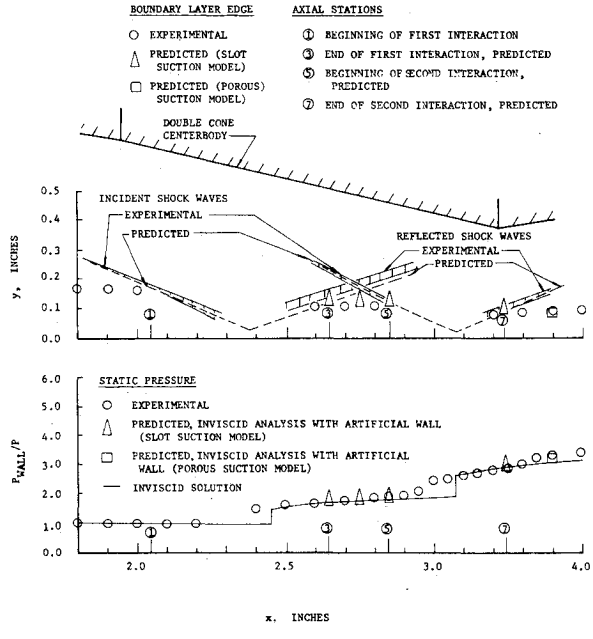

Fig. 9 Shock wave positions, boundary-layer thicknesses and wall static pressures, $M_\infty = 2.82$, 5.0% bleed.

For the Mach 2.82 flow with bleed, the bleed models described under Step 1) and depicted schematically in Figs. 3a and 3b were used. The bleed holes used in the study were drilled normal to the wind-tunnel wall. At first thought, then, the porous-wall model might appear to provide a better representation of the bleed flow. However, the bleed-hole diameter of 0.052 in. was on the order of one-half the boundary-layer thickness at Station 5. Thus, there should be x-momentum associated with the bleed flow and the bleed flow behavior might then be expected to lie somewhere between that for porous-wall suction and slot suction. As will be discussed in the section on results, this appears to have been the case.

Results

The results of the analysis are shown in Figs. 4–11. Comparisons are made between predicted and measured results. The data for the $M_\infty = 2.82$ flow are from an investigation by Teeter.[7]

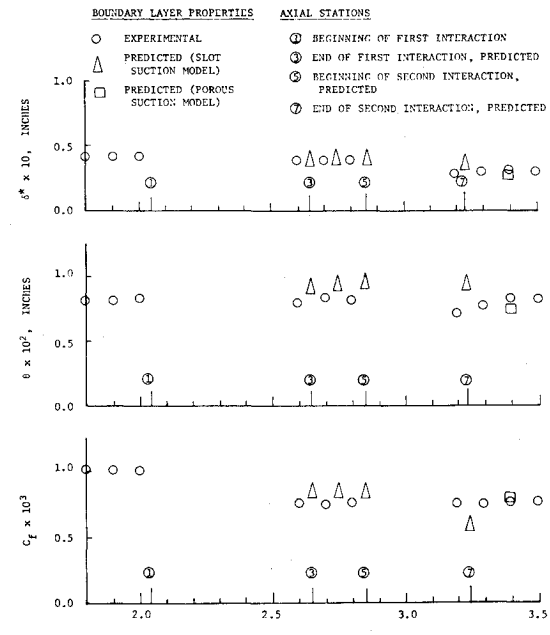

Fig. 10 δ^*, θ, C_f, $M_\infty = 2.82$, 5.0% bleed.

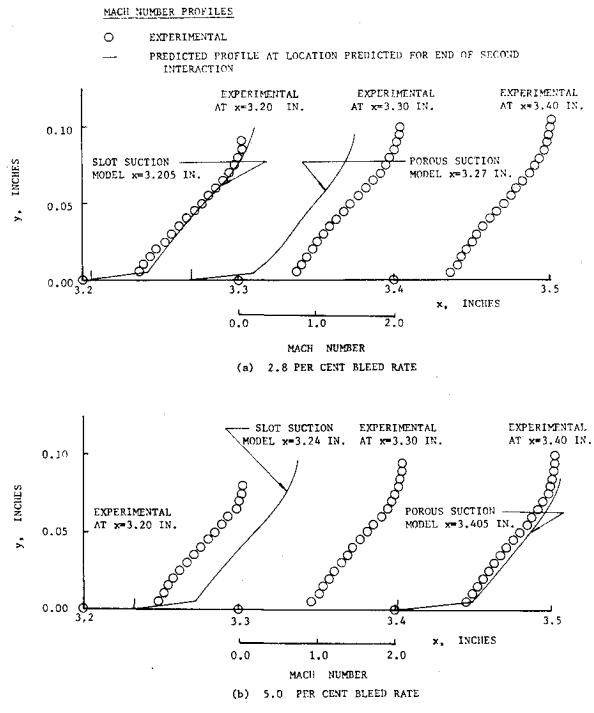

Fig. 11 Mach number profiles downstream of second interaction, $M_\infty = 2.82$, 2.8% bleed, 5.0% bleed.

Figure 4 shows comparisons of the experimental and predicted shock wave patterns and boundary-layer thicknesses for the Mach 3.82 flow. Since the predicted shock wave locations are determined by the inviscid analysis used in combination with the artificial wall position, no induced shock wave is predicted. Also shown is the pressure distribution at the tunnel side wall as a function of the distance aft of the cone tip. The triangular points shown for the analysis in the static pressure plot were determined by using the artificial wall and the inviscid flow solution. The predicted and observed values are seen to be in good agreement along the entire length of the double-shock interaction.

Figure 5 shows δ^*, θ, and C_f at several stations along the tunnel side wall. Here, also, predicted and observed results are in good agreement. The experimental values

shown for C_f have been determined by a least-squares fit of the modified wall-wake velocity profile to the experimentally determined velocity profiles.

Figure 6 shows Mach Number profiles for the boundary layer at the downstream end of the second interaction. The analysis predicts the end of the second interaction to be at $x = 3.75$ in. Since profiles were not taken at this specific station, profiles taken just upstream, $x = 3.70$ in., and just downstream, $x = 3.80$ in., are shown for comparison. It is apparent that the analysis leads to a profile which provides a good representation of the experimentally determined profiles near the interaction end.

Figure 7 shows boundary-layer thicknesses, shock wave patterns and wall static pressure distributions for the Mach 2.82 flow with 2.8% boundary-layer bleed at the second interaction site. Figure 8 shows δ^*, θ, and C_f for this flow.

Two sets of predicted results are given, one for the porous-wall suction model, the other for slot suction. As is shown, the differences between the results for the two suction models are not large. Differences in predicted results with the two models are due solely to the differences in values assigned to the x-momentum of the bleed flux. Since the bleed rate is low, the x-momentum associated with the slot suction model is small and not too different from the zero values for porous suction. The predicted and measured results are in reasonably good agreement.

Figure 9 shows boundary-layer thicknesses, shock wave patterns and wall static pressure distributions for $M = 2.82$ with 5.0% bleed. Values for δ^*, θ, and C_f are shown in Fig. 10, while Mach Number profiles downstream of the second interaction are shown in Fig. 11. The Mach Number profiles represented by the solid lines in Fig. 11 are predicted profiles for the two bleed flow models. They are shown on the figure at the axial positions predicted for the end of the second interaction. Since experimental profiles were not taken at these precise locations, experimental profiles taken in the neighborhood ($x = 3.20$, 3.30, and 3.40 in.) of the predicted locations have been shown for comparison.

The flow conditions up to the second interaction are the same as those for the flow with 2.8% bleed. With the higher bleed rate the difference between the results for porous wall and slot suction are much more pronounced than with 2.8% bleed. The slot-suction model gives a reflected shock location which is in better agreement with the observed results. On the other hand, the values of δ^*, θ, and C_f obtained with the porous wall model agree better with experimental values than do the slot suction results. As was pointed out in the section on analysis, the bleed hole diameter of 0.052 in. was on the order of one-half of the boundary-layer thickness so that the bleed flow behavior might be expected to lie between that for porous wall suction and slot suction. The x-momentum of the bleed value might then, in turn, be expected to lie between the values used with the two models. Indeed, the use of a bleed flow momentum flux between the two limits would lead to better over-all agreement between predicted and measured values of δ^*, θ, and C_f. Even then, however, the predicted interaction length would be too long. It should be remarked that in estimating I_{Bx} for the slot-suction bleed flow model, no allowance is made for the turbulent shear stress along the stream surface separating the bleed flow from the main body of the flow, nor for the wall shear stress. Nor is the pressure force along the separating stream surface considered. The effects of the pressure force and wall shear tend to cancel the effect of the turbulent shear on the separating stream surface, but the extent to which they do so is not known. It should be remarked further that no allowance is made for the roughness effect of the holes on the wall shear. Further study is needed on the details of the bleed flow behavior, including the roughness effect of the holes, before the effects of bleed configuration can be resolved.

The computation procedure reported here represents the results of a continuing effort to improve analytical methods of predicting flowfields in the inlets of supersonic aircraft. In a recent analysis of inlet flowfields by Reyhner and Hickcox[8] the effect of the shock wave interaction on the inviscid flow was taken into account by first obtaining a control volume solution for the boundary-layer properties downstream of the interaction. Then, using an effective surface defined by the boundary-layer displacement thicknesses upstream and downstream of the interaction, and using a patching technique across the interaction region to construct an effective displacement surface for that region, the inviscid flow solution was obtained for the effective surface. A comparable technique was tried in the work reported here but it was not as successful as the scheme of using the simple reflection off the artificial wall.

Conclusions

A control volume analysis method, employed in conjunction with a turbulent boundary-layer computation scheme, has been used to predict the flowfield downstream of successive shock wave boundary-layer interactions for flows at $M_\infty = 3.82$ and 2.82. The effects of boundary layer bleed at the second interaction site have been considered. For flow with low bleed rates or no bleed the predicted interaction lengths, and wall static pressures, as well as the boundary-layer properties downstream of the interactions show good agreement with measured results. With low bleed flow the predicted results for the slot-suction and porous-wall models differ only slightly since the momentum of the bleed flow is small. As the bleed flow rate is increased, predicted and measured results are also in reasonably good agreement. Here, however, differences between predicted results for the two suction models are larger since the difference between the momentum fluxes of the bleed flows is larger. A value of bleed flow momentum between the values used for the models would improve the agreement between predicted and measured results.

References

[1]Seebaugh, W. R., Paynter, G. C., and Childs, M. E., "Shock-Wave Reflection from a Turbulent Boundary Layer with Mass Bleed," *Journal of Aircraft*, Vol. 5, No. 5, Sept.–Oct. 1968, pp. 461–467.

[2]Mathews, D. C. "Shock Wave-Boundary Layer Interactions in Two-Dimensional and Axially Symmetric Flows Including the Influence of Suction," Ph.D. thesis, 1969, Dept. of Mechanical Engineering, University of Washington, Seattle, Wash.

[3]Mathews, D. C., Childs, M. E., and Paynter, G. C., "Use of Coles' Universal Wake Function for Compressible Turbulent Boundary Layer," *Journal of Aircraft*, Vol. 7, No. 2, March–April 1970, pp. 137–140.

[4]Sun, C. C. and Childs, M. E., "A Modified Wall-Wake Velocity Profile for Turbulent Compressible Boundary Layers," *Journal of Aircraft*, Vol. 10, No. 6, June 1973, pp. 381–383.

[5]Paynter, G. C. and Schuehle, A. L., private communication, 1971, The Boeing Company, Seattle, Wash.

[6]Green, J. E., "The Prediction of Turbulent Boundary Layer Development in Compressible Flow," *Journal of Fluid Mechanics*, Vol. 31, Pt. 4, 1968, pp. 753–778.

[7]Teeter, G. C., "An Experimental Investigation of the Interaction of a Shock Wave with a Decelerated Turbulent Boundary Layer," M. S. thesis, 1971, Dept. of Mechanical Engineering, University of Washington, Seattle, Wash.

[8]Reyhner, T. A. and Hickox, T. E., "Combined Viscous-Inviscid Analysis of Supersonic Inlet Flowfields," *Journal of Aircraft*, Vol. 9, No. 8, Aug. 1972, pp. 589–595.